IOP Publishing Physica Scripta
Phys. Scr. 95 (2020) 045102 (7pp) https://doi.org/10.1088/1402-4896/ab6523

Modeling two-qubit Grover's algorithm implementation in a linear optical chip

E Samsonov[1], F Kiselev[1,2], Y Shmelev[1], V Egorov[1], R Goncharov[1], A Santev[1], B Pervushin[1] and A Gleim[1]

[1] ITMO University, Kronverkskiy, 49, St.Petersburg, 197101, Russia
[2] Corning Research & Development Corporation, Corning, NY, United States of America

E-mail: edi.samsonov@gmail.com

Received 17 July 2019, revised 7 December 2019
Accepted for publication 23 December 2019
Published 14 February 2020

Abstract

This paper introduces a model of Grover's algorithm suitable for implementation in a linear photonic chip. We compare two known realizations of its main components, two-qubit CZ gates, in order to define optimal chip architecture. The algorithm operation is simulated considering directional coupler imperfection influence on the scheme parameters. We also determined tolerance boundaries for distortions of the coupler dimensions.

Keywords: quantum computing, Grovers algorithm, optical chip, linear optical quantum computing

(Some figures may appear in colour only in the online journal)

1. Introduction

Optical systems that use photonic degrees of freedom play a key role in quantum information science and communication. During the ultimate decade scientists proposed optical implementations of all basic quantum computing operations, including Grover's search and Shor's quantum factoring algorithms [1, 2]. Another actively studied direction in optical quantum computing is boson sampling [3].

Until recently photonic quantum computing demonstrations have been realized using bulk optical elements [4]. Because of their large size and inherent instability this approach hinders the development of scalable quantum computing systems. A promising way of solving this problem is using integrated photonic schemes composed of linear optical elements (directional couplers (DCs) and phase shifters). Recently the authors of [5] demonstrated the possibility of creating large-scale quantum photonic chip using various materials. Paper [6] describes a six-mode universal system integrated into a single photonic chip that is sufficient to implement all possible linear optical protocols up to the size of that circuit.

Universal quantum computing system is an optical circuit that would allow to reconstruct any quantum algorithm using unitary transformations of the quantum information carriers. Unfortunately, in a realistic scenario such approach overcomplicates the scheme leading to increasing number of errors and lower fidelity. For example, Mach–Zehnder interferometer—key element of universal optical quantum computation—increases optical length of the chip and makes it more expensive in comparison with regular DC that could be used instead if universality is not required. An alternative lies in development of a specific quantum circuits for solving certain problems. A specially designed chip will have significantly fewer distortions than the universal system making such implementation more efficient. For example, Grover's algorithm single chip implementation can be useful in quantum networking for the purposes of calculating optimal signal routing [7–9]. The Grover's algorithm based on bulk optics has been offered to date [10]. However, an algorithm model suitable for realization in an optical chip has not been proposed yet.

Both bulk and on-chip implementations have several common limitations. The bottleneck of any quantum computing system is a two-qubit gate. For instance, Grover's algorithm implementation requires at least two of them. Optical two-qubit gate implementation is limited because of weak photon-photon interaction [11]. In order to to solve this problem, linear optical quantum computation (LOQC) protocols were developed. Today it is possible to create a full set of universal unitary gates using linear optical elements [12]. Knill, Laflamme, and Milburn (KLM) showed that a two-qubit gate

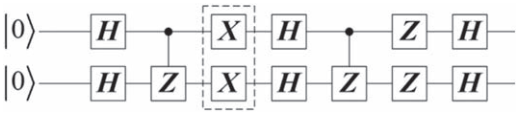

Figure 1. Grover's algorithm scheme. When **II** (two-qubit identity gate) is applied in the dashed box, state $|11\rangle$ is marked. Similarly one can apply **XI** for marking $|01\rangle$, **IX** for $|10\rangle$, **XX** for $|00\rangle$.

can be constructed using linear optical elements, auxiliary photons, and measurement [13]. In their paper, KLM proposed a probabilistic **CNOT** with success probability $P = 1/16$. This probability can be increased further if its gates generate entangled states used as a resource for the implementation of a controlled unitary operation based on quantum teleportation [13]. Later an alternative **CNOT** gate implementation with $P = 1/9$ was presented in [14]. It uses two photons and two auxiliary modes (a two-photon CZ gate). Theoretical study of correlations between perturbations of two-photon **CNOT** circuit parameters and its performance was given in [15]. Both of these gates have been demonstrated experimentally on optical chips [6, 16, 17]. Other limiting factors of optical realizations of quantum algorithms include propagation and coupling losses, photon generation and detection efficiency and imperfections of the optical scheme. The latter include fabrication inaccuracy of DCs and phase shifters and dark counts of photon detectors.

In this work we propose a Grover's algorithm model that can be implemented in an integrated optical waveguide circuit. We consider using two above mentioned **CNOT** realizations and choose the optimal one. We also simulate the algorithm taking DC imperfections into consideration. To determine the tolerance for direction coupler technological parameters, we simulate algorithm operation with DC distortions in length and separation of the central coupling region. In the end we investigate how the proposed circuit scales with a larger number of qubits.

2. The Grover's algorithm in LOQC

The Grover's algorithm identifies one of N elements, marked by an oracle, with order $\sqrt{N}$ uses of the oracle [18]. The search problem can be represented by function $f(x) = 1$ if x is a solution, otherwise $f(x) = 0$. The quantum oracle, represented by unitary operator **O**, recognizes solutions to the problem. Detailed algorithm description can be found in [11]. Here we consider a simplified quantum circuit of the algorithm (figure 1) which allows us to reduce the number of errors sources. The scheme consists of the following unitary operators: **X**, **Z** are Pauli gates, **I** is identity gate, **CZ** is controlled Pauli **Z**, and **H** is Hadamard gate. Here we substitute **CNOT** with **CZ**, using **CNOT** $= (\mathbf{I} \otimes \mathbf{H})(\mathbf{CZ})(\mathbf{I} \otimes \mathbf{H})$ and reducing the Hadamard gates. In the classical Grover's circuit [11] the oracle uses an auxiliary qubit, while in this proposed circuit the oracle is performed by a combination of **CZ** and **X**. The marked state is specified inside the oracle, it is defined by whether the **X** gates (in the dashed box) are applied. Thus, if the marked state is $|10\rangle$ after oracle we get $(\mathbf{I} \otimes \mathbf{X})\mathbf{CZ}|\phi\rangle = |00\rangle + |01\rangle - |10\rangle + |11\rangle = |\psi\rangle$ (omitting the normalization). The next part of the scheme is equivalent to the inversion operator $(\mathbf{H} \otimes \mathbf{H})(\mathbf{Z} \otimes \mathbf{Z})\mathbf{CZ}$ $(\mathbf{H} \otimes \mathbf{H})|\psi\rangle = |10\rangle$, hence we find the marked state $|10\rangle$.

Table 1. Quantum gates and their linear optical implementations.

Quantum gates	Linear optical implementations
$\mathbf{Z} = \begin{pmatrix} 1 & 0 \\ 0 & -1 \end{pmatrix}$	Phase delay $\phi = \pi$
$\mathbf{X} = \begin{pmatrix} 0 & 1 \\ 1 & 0 \end{pmatrix}$	DC with transmission coefficient $T = 1$
$\mathbf{I} = \begin{pmatrix} 1 & 0 \\ 0 & 1 \end{pmatrix}$	DC with transmission coefficient $T = 0$
$\mathbf{H} = \frac{1}{\sqrt{2}}\begin{pmatrix} 1 & 1 \\ 1 & -1 \end{pmatrix}$	DC with transmission coefficient $T = 0.5$ (up to phase factors), figure 2
$\mathbf{U} = \begin{pmatrix} \cos\phi/2 & \sin\phi/2 \\ \sin\phi/2 & \cos\phi/2 \end{pmatrix}$	Mach–Zehnder interferometer, ϕ is phase shift 0 or π
$\mathbf{CZ} = \begin{pmatrix} 1 & 0 & 0 & 0 \\ 0 & 1 & 0 & 0 \\ 0 & 0 & 1 & 0 \\ 0 & 0 & 0 & -1 \end{pmatrix}$	Two-qubit in accordance with LOQC protocols

To represent a qubit we use spatial mode separation approach (dual-rail encoding). Such schemes consist of several conventional optical elements, i.e. phase shifters and DCs. The Hamiltonian of a phase shifter is:

$$\mathbf{H}_{\text{phi}} = \phi \hat{a}^{\dagger}_{\text{in}} \hat{a}_{\text{in}},$$
$$\hat{a}^{\dagger}_{\text{out}} = e^{i\phi \hat{a}^{\dagger}_{\text{in}} \hat{a}_{\text{in}}} \hat{a}^{\dagger}_{\text{in}} e^{-i\phi \hat{a}^{\dagger}_{\text{in}} \hat{a}_{\text{in}}} = e^{i\phi} \hat{a}^{\dagger}_{\text{in}}, \quad (1)$$

where $\hat{a}^{\dagger}$, $\hat{a}$ are creation and annihilation operators $[\hat{a}^{\dagger}, \hat{a}] = 1$, $[\hat{a}, \hat{a}] = 0$, $[\hat{a}^{\dagger}, \hat{a}^{\dagger}] = 0$. $|n\rangle = (n!)^{-1/2}(\hat{a}^{\dagger})^n|0\rangle$ is a Fock state with n photons. $|0\rangle$ is a vacuum state, and $|1\rangle$ is a single-photon state. DC Hamiltonian is:

$$\mathbf{H}_{\text{BS}} = \theta e^{i\phi} \hat{a}^{\dagger}_{\text{in}} \hat{b}_{\text{in}} + \theta e^{-i\phi} \hat{a}_{\text{in}} \hat{b}^{\dagger}_{\text{in}}, \quad (2)$$

DC input and output ratio in the operator form are given as:

$$\hat{a}^{\dagger}_{\text{out}} = \cos\theta \hat{a}^{\dagger}_{\text{in}} + ie^{-i\phi} \sin\theta \hat{b}^{\dagger}_{\text{in}}$$
$$\hat{b}^{\dagger}_{\text{out}} = ie^{i\phi} \sin\theta \hat{a}^{\dagger}_{\text{in}} + \cos\theta \hat{b}^{\dagger}_{\text{in}}. \quad (3)$$

Here reflection and transmission coefficients are $R = \sin^2\theta$, $T = 1 - R = \cos^2\theta$, respectively. One-qubit gates used for modeling the scheme and their implementations in dual-rail encoding LOQC are given in table 1. The phase factor provides a unitary transformation.

Using these elements we can construct an optical implementation of the circuit in figure 1. The resulting circuit is shown in figure 2. A detailed scheme of Hadamard gate is in figure 3. In order to prepare a superposition, the input state is set to $|00\rangle$, which is equivalent to $|1010\rangle$ in dual-rail encoding Fock state. Optimal **CZ** gate will be chosen in the following section.

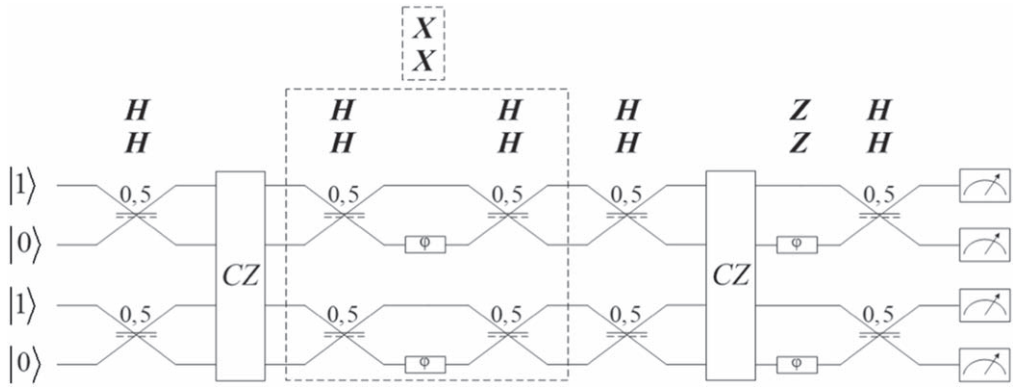

Figure 2. Optical realization of Grover's algorithm. The numbers indicate the reflection coefficients R, the dashed line denotes phase sign change. Directional couplers at the end of the Mach–Zehnder interferometers can be omitted, since (**HH** = **I**).

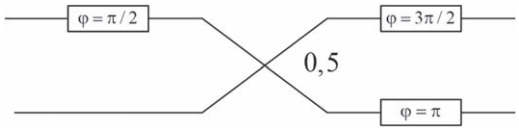

Figure 3. Detailed scheme of a linear optical Hadamard gate.

3. Optimal implementation of a two-qubit CZ gate

The scheme in figure 2 contains two **CZ** gates, their matrix form is given in table 1. It is possible to use one of the two existing LOQC implementations, two-phonon CZ and KLM CZ (see section 1).

3.1. Two-photon CZ gate

Let us first consider a two-photon **CZ** gate, which has relatively high probability ($P = 1/9$). LOQC Grover's algorithm possible implementation with a two-photon **CZ** gate is given in figure 4.

In this paper we show that the two-photon **CZ** gate is not valid option for performing the algorithm. Let us prove this statement by calculating a state at the scheme output if for example a state $|01\rangle$ is marked. Let the input state be:

$$|\phi\rangle = c_1^\dagger t_1^\dagger, \tag{4}$$

where $c_1^\dagger$ and $t_1^\dagger$ are creation operators for the first control and target modes consistently. According to (equation (3)), the equations for **CZ** gate relating the control (C) and the target (T) input modes to their corresponding outputs are:

$$C_{1\text{out}} = \frac{1}{\sqrt{3}}(C_1 + \sqrt{2}\,v_c), \tag{5}$$

$$C_{2\text{out}} = \frac{1}{\sqrt{3}}(-C_2 + \sqrt{2}\,T_1), \tag{6}$$

$$T_{1\text{out}} = \frac{1}{\sqrt{3}}(\sqrt{2}\,C_2 + T_1), \tag{7}$$

$$T_{2\text{out}} = \frac{1}{\sqrt{3}}(T_2 + \sqrt{2}\,v_t). \tag{8}$$

Relating equation for one-qubit gates are described by (equations (1), (2)). The operators are applied to the state in (equation (4)) successively according to the linear algebra laws. Superposition state before a first **CZ** gate is:

$$|\psi_1\rangle = \frac{1}{2}(c_1^\dagger t_1^\dagger + c_1^\dagger t_2^\dagger + c_2^\dagger t_1^\dagger + c_2^\dagger t_2^\dagger)|0000\rangle. \tag{9}$$

Then the state after the first **CZ** gate is:

$$|\psi_2\rangle = \frac{1}{6}(c_1^\dagger t_1^\dagger + c_1^\dagger t_2^\dagger + c_2^\dagger t_1^\dagger - c_2^\dagger t_2^\dagger + \sqrt{2}\,c_2^\dagger c_2^\dagger + \sqrt{2}\,t_1^\dagger t_1^\dagger + \sqrt{2}\,c_1^\dagger c_2^\dagger + \sqrt{2}\,t_1^\dagger t_2^\dagger + \text{ext})|0000\rangle. \tag{10}$$

After post-selection we can neglect some external states when there is photon in auxiliary mode. But the other external states will contribute to the error because we do not perform a measurement right after the first **CZ** gate. As a result, the output state after a second part of the algorithm is given by:

$$|\psi_{\text{out}}\rangle = \frac{1}{9}(-2|1010\rangle - 2|1001\rangle + |0110\rangle + 2|0101\rangle + \text{ext}). \tag{11}$$

We can see that the Grover's algorithm with 1/9-probability **CZ** gate does not allow to identifies the marked state because of the two-photon gate error. We find from the calculations that even if we change the Grover's circuit design the two-photon **CZ** gate will contribute the critical error in the algorithm work.

3.2. KLM CZ gate

Now we shall analyze the KLM **CZ** gate, which allows to avoid the errors of the previous one. The reason for this is that in KLM gate a successful operation is heralded by two of the four detectors, and the gate flips the sign of the $|11\rangle$ state probability amplitude [12]. Hence we know exactly when the operation was successful and can use two gates consequentially. The only practical limitation of this operator is low probability ($P = 1/16$). Even though there are methods of increasing it, here we consider the simplest implementation of the protocol. KLM gate significantly reduces Grover's algorithm efficiency but allows it to proceed without mistakes. There already exist implementations of two-qubit gates

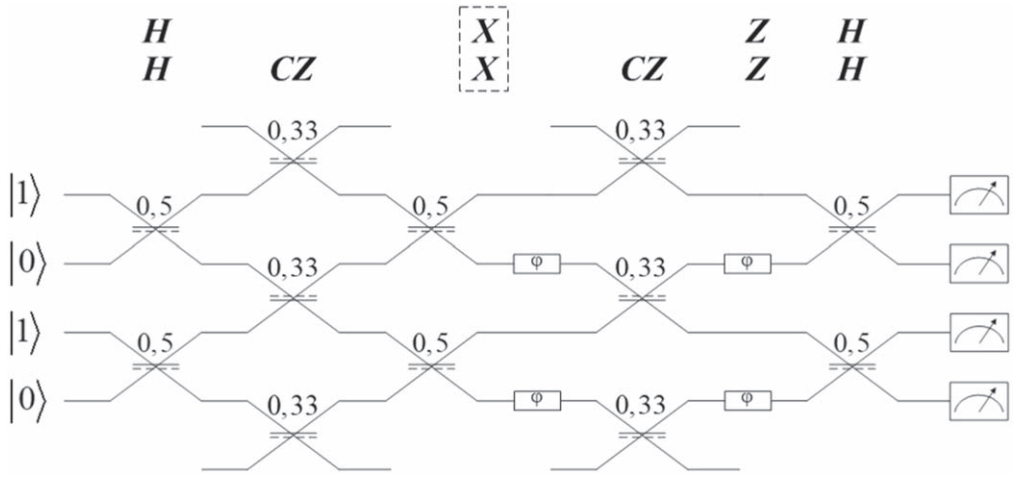

Figure 4. LOQC Grover's algorithm implementation with two-photon **CZ** gate.

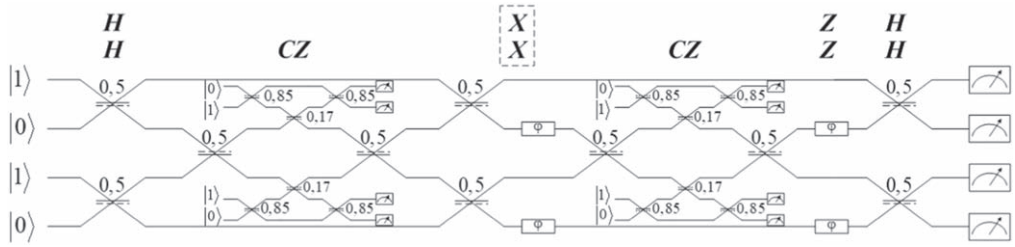

Figure 5. LOQC Grover's algorithm implementation with two-cubit KLM gate.

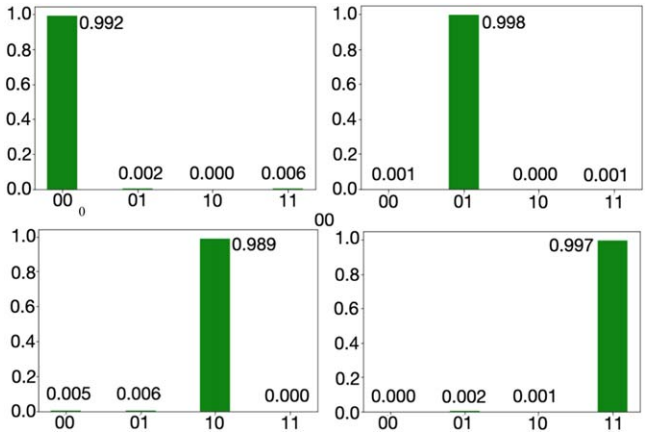

Figure 6. Simulating result of the Grover's algorithm with coupler splitting coefficients randomly tilted in range (0.5 ± 0.034).

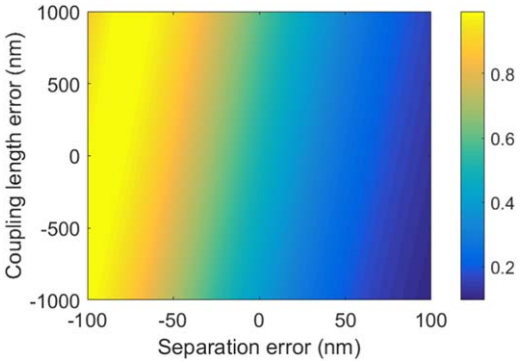

Figure 7. Splitting coefficient variation depending on separation and coupling length errors. Center of the figure corresponds to an ideal case with splitting coefficient of 0.5.

with projections measurements and post-selection in bulk with polarization qubits [19] and on an optical chip [20]. Authors achieved fidelities close to unity. In this paper we propose to use KLM CZ gate in optical implementation of Grover's algorithm. This approach is similar to one shown in [20], however we do not aim to make the chip universal and fully re-configurable. We suggest that such simplified chips can be used to perform sub-routines of more complex problems. The final version of proposed scheme for algorithm implementation with KLM CZ gates is given in figure 5.

4. Algorithm simulation in presence of DC distortions

Now let us consider errors in the algorithm that appear due to DC dimensional inaccuracy that always remains an issue during fabrication process. A DC is a key element of LOQC, and its imperfections make a significant contribution to error rate in one-qubit linear optical gates [21, 22]. We present simulation results of the algorithm implementation given in figure 2 with errors introduced by direction coupler parameter deviations. Here we consider only errors from single-qubit

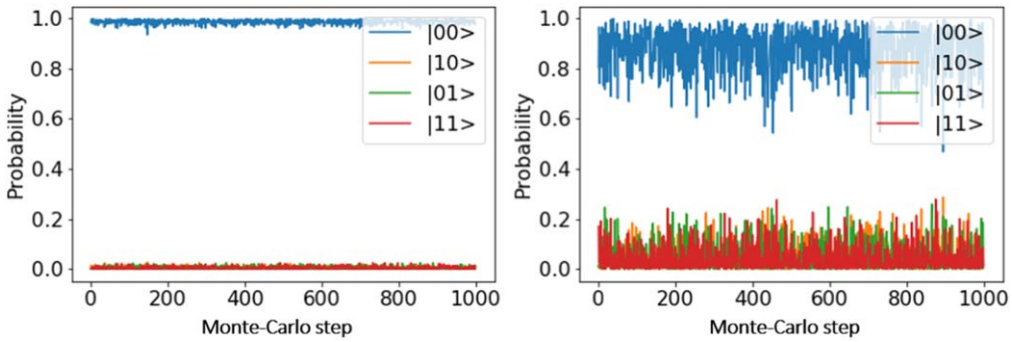

Figure 8. State identification probability during N runs of Grover's algorithm, the marked state is $|00\rangle$. Commentary is given in the text.

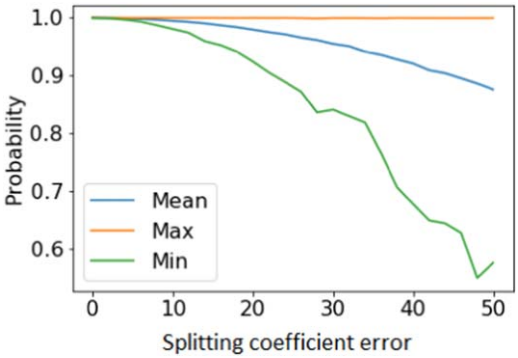

Figure 9. Minimum (blue), maximum (orange) and mean (green) success probabilities obtained from Monte-Carlo simulations for different splitting coefficient errors.

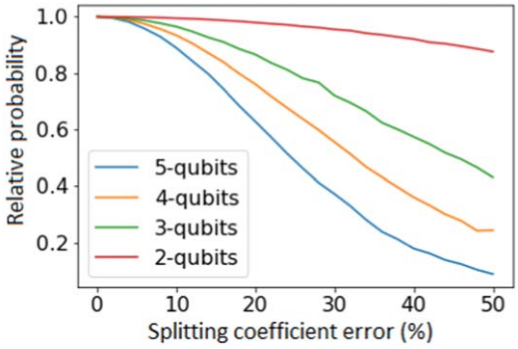

Figure 10. Mean success probabilities of Grover's algorithm with different qubit count.

gates, assuming that KLM gate works perfectly when the photons are detected in respective ancillary channels.

In order to fully estimate algorithm errors one should also consider single-photon sources and detectors. It is known that the output success probability of a source above 0.7 and the total system (optics and detectors) efficiency above 0.9 will allow to achieve performing simple KLM gate without post-selection [23]. Current LOQC experiments require extensive post-selection and long measurement times and involve only about six photons. Full description of the algorithm work should include simulating single-photon devices, which will be done in future works.

For our simulations we used the parameters of existing silica-on-silicon DCs [21]. Modeling was performed using QuTiP library [24] in Python. Figure 6 presents and example of simulation results for a splitting coefficient error ± 0.034, showing the output states for each marked state. It can be seen that error probability does not exceed 0.011.

Coupler dimensions that contribute the most to error rate are its length and waveguide separation in the coupling region [25]. To determine the conditions under which the algorithm operates stably we performed a simulation varying both parameters.

We began with calculating silica-on-silicon DC splitting coefficient for different values of length and separation distortions using finite element method (FEM) in Matlab mode solver [26]. We used exponential approximation to describe coupling length as a function of separation. The splitting coefficient C can be written as:

$$C(\Delta l, \Delta s) = \sin^2(a(L_{\text{int}} + l_0 + \Delta l)\mathrm{e}^{(-(s+\Delta s)/\tau)}), \quad (12)$$

where L_{int} is the coupling region length, l_0 is effective coupling length of the transition region, s is separation between two waveguides in the coupling region, Δl and Δs are distortions of coupling length and separation, respectively. Symbols a and τ denote approximation parameters obtained from FEM simulation, their values are 1.05×10^{-3} and 129.15, respectively. Values of coupling region length and separation were chosen so that C is equal to 0.5 in zero errors. For silica-on-silicon waveguides these values are $L_{\text{int}} + l_0 = 7650$ nm and $s = 300$ nm. Equation (12) gives us a map of splitting coefficient values depending on dimensional errors (figure 7). In order to observe the effect of distortions on in the Grover's algorithm, we applied the splitting deviations calculated for different values of Δl and Δs into Hadamard matrices.

According to (equation (3)), unitary operator for Hadamard gate with an arbitrary DC can be calculated as:

$$\mathbf{H}(C) = \begin{pmatrix} -\mathrm{i} & 0 \\ 0 & -1 \end{pmatrix} \begin{pmatrix} \sqrt{1-C} & \mathrm{i}\sqrt{C} \\ \mathrm{i}\sqrt{C} & \sqrt{1-C} \end{pmatrix} \begin{pmatrix} \mathrm{i} & 0 \\ 0 & 1 \end{pmatrix} = \begin{pmatrix} \sqrt{1-C} & \sqrt{C} \\ \sqrt{C} & -\sqrt{1-C} \end{pmatrix}. \quad (13)$$

By replacing the ideal splitting coefficient with a distorted one we get a Hadamard gate with distortions. To simulate these distortions we used Monte-Carlo approach, randomly choosing

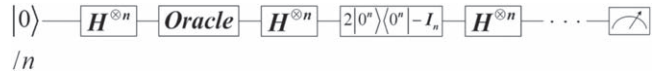

Figure 11. *n*-qubit Grover's algorithm circuit.

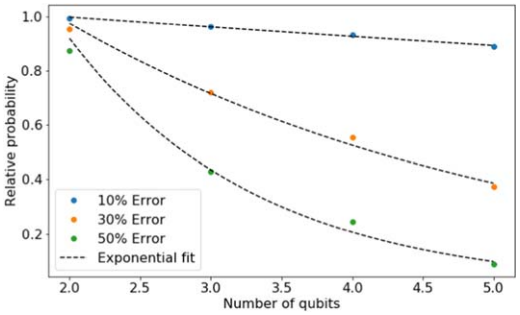

Figure 12. Relative probabilities of Grover's algorithm versus its qubit count plotted for different rates of splitting coefficient error and fitted by an exponential function.

splitting coefficient for every Hadamard gate in a single step within boundaries which correspond to a certain set of distortion values.

Figure 8 illustrates the algorithm success probability for $N = 1000$ Monte-Carlo steps for two different levels of splitting coefficient distortion. The marked state is $|00\rangle$. On the left graph splitting coefficient error is $\pm 16\%$ corresponding to $\Delta l = \pm 100$ nm and $\Delta s = \pm 10$ nm. On the right graph the error is $\pm 50\%$, $\Delta l = \pm 350$ nm and $\Delta s = \pm 30$ nm. For other marked states the results show similar behavior.

This model gives us performance estimation for the proposed Grover's algorithm realization on a photonic chip. We performed simple statistical analysis of data obtained from Monte-Carlo simulations for different values of splitting coefficient error. Note that for every point of splitting coefficient error in this data has a form shown in figure 8. Figure 9 shows minimum, mean and maximum values of algorithm success probabilities obtained from these simulations as functions of splitting coefficient error. One can see that while minimal success probability drops fast, the mean value declines much slower and does not fall below 0.95. Similar performance was achieved for two-qubit quantum processor in [20]. This indicates that in a lot of cases the algorithm works even for very large errors. Situation changes if we consider higher number of qubits. In this paper we also consider Grover's algorithm schemes with larger qubit count—3, 4 and 5 qubits. It is known that scalability is one of the main challenges for LOQC as well as for other physical implementations. We can construct *n*-qubit Grover's algorithm according to figure 11. We simulated these schemes using the same approach and looked at the mean success probabilities of each (figure 10). As one can see mean probabilities drop much faster with the increase of qubit count. During the calculation we found that success probabilities for some cases are not exactly equal to 1. To create a fair comparison we considered probabilities relative to the ideal case of respective qubit count. We also plotted success probabilities versus the qubit count and fitted it with the decreasing exponential (figure 12). It is hard to see the exponential decay for the case of 10% error rate however if we move to higher rates (30% and 50%) we can see the trend more clear. This approximation can be used to estimate decrease of success probabilities for Grover's algorithm with qubit count much larger than classical computer could simulate. For example if we consider 50-qubit Grover's algorithm with the 10% error rate we get the estimate value of success probability equal to 0.17. We want to note that 10% error rate could correspond to dimensional errors of DCs based on Si_3N_4 calculated in [25].

5. Conclusion

We proposed two-qubit Grover's algorithm optical scheme which can be integrated into a chip. Our analysis shows that it is necessary to use KLM CZ gates instead of two-photon CZ gates with higher success probability, due to mode matching errors of the latter. Also, in general it is more preferable to use gates with projection measurements as it allows for post-selection of the output and thus allows for mitigation of two-qubit gate errors that come from probabilistic nature of LOQC. We modeled the algorithm performance taking into consideration DC distortions in Hadamard gates. Finally we determined algorithm tolerances against distortions in technological parameters of DCs. Our analysis shows that mean success probability scales slowly with error splitting ratio and does not fall below 0.8 for two-qubit algorithm. However, mean probability begin to drop much faster if we consider higher number of qubits. We calculated mean success probabilities of 3, 4 and 5-qubit Grover's algorithm. Our analysis shows that success probabilities attenuate exponentially. This trend can be considered as a scalability problem with respect to dimensional errors of DCs in LOQC.

Acknowledgments

This work was financially supported by Government of Russian Federation (Grant 08-08) and Russian Ministry of Education (Grant No. 2020-0903).

ORCID iDs

R Goncharov https://orcid.org/0000-0002-9081-8900

References

[1] Politi A, Matthews J C F and O'Brien J L 2009 Shor's quantum factoring algorithm on a photonic chip *Science* **325** 1221
[2] Kwiat P, Mitchell J, Schwindt P and White A 2002 Optical implementation of Grover's algorithm: it's all done with mirrors *Quantum Communication Computing and Measurement 2* (Boston: Springer)
[3] Gard B T, Motes K R, Olson J P, Rohde P P and Dowling J P 2015 An introduction to Boson-sampling *From Atomic to Mesoscale: The Role of Quantum Coherence in Systems of Various Complexities* (Singapore: World Scientific) ch 8

[4] Thompson M G, Politi A, Matthews J C F and O'Brien J L 2011 Circuits for optical quantum computing IET circuits *Devices Syst.* **5** 94–102
[5] Harris N C, Bunandar D, Pant M, Steinbrecher G R, Mower J, Prabhu M, Baehr-Jones T, Hochberg M and Englund D 2016 Large-scale quantum photonic circuits in silicon *Nanophotonics* **5** 456–68
[6] Carolan J *et al* 2015 Universal linear optics *Science* **349** 711–6
[7] Meng L and Song W 2013 Routing protocol based on Grover's searching algorithm for Mobile Ad-hoc *Netw. China Commun.* **10** 145–56
[8] Mariappan H, Kaliappan M and Vimal S 2016 Energy efficient routing protocol using Grover's searching algorithm for MANET Asian *J. Inf. Technol.* **15** 4986–94
[9] Reza M, Aghaei S, Zukarnain A, Mamat A and Zainuddin H 2013 A hybrid algorithm for finding shortest path in network Routing *Int. J. Multimedia Ubiquitous Eng.* **8** 360–5
[10] Dodd J L, Ralph T C and Milburn G J 2003 Experimental requirements for Grover's algorithm in optical quantum computation *Phys. Rev.* A **68** 042328
[11] Nielsen M A and Chuang L I 2000 *Quantum Computation and Quantum Information* (Cambridge: Cambridge University Press)
[12] Kok P, Munro W J, Nemoto K, Ralph T C, Dowling J P and Milburn G J 2007 Linear optical quantum computing with photonic qubits *Rev. Mod. Phys.* **79** 135
[13] Knill E, Laflamme R and Milburn G J 2001 A scheme for efficient quantum computation with linear optics *Nature* **409** 46–52
[14] Ralph T C, Langford N K, Bell T B and White A G 2002 Linear optical controlled-NOT gate in the coincidence basis *Phys. Rev.* A **65** 062324
[15] Kozubov A V and Chivilikhin S A 2015 Theoretical investigation of the correlation between perturbations of quantum optical circuit parameters and its performance *J. Phys.: Conf. Ser.* **643** 012060
[16] Okamoto R, O'Brien J L, Hofmann H F and Takeuchi S 2011 Realization of a Knill–Laflamme–Milburn controlled-NOT photonic quantum circuit combining effective optical nonlinearities *Proc. Natl Acad. Sci.* **25** 10067–71
[17] O'Brien J L, Pryde G J, White A G, Ralph T C and Branning D 2003 Demonstration of an all-optical quantum controlled-NOT gate *Nature* **426** 264–7
[18] Grover L K 1996 Quantum mechanics helps in searching for a needle in a haystack *Phys. Rev. Lett.* **79** 212–9
[19] Barz S, Kassal I, Ringbauer M, Lipp Y O, Dakic B, Aspuru-Guzik A and Walther P 1996 A two-qubit photonic quantum processor and its application to solving systems of linear equations *Sci. Rep.* **4** 6115
[20] Qiang X *et al* 2018 Large-scale silicon quantum photonics implementing arbitrary two-qubit processing *Nat. Photon.* **12** 534
[21] Politi A, Matthews J, Thompson M J and O'Brien J L 2009 Integrated quantum photonics *IEEE J. Sel. Top. Quantum Electron.* **15** 1673–84
[22] Vasilev A, Kozubov A, Gaidash A and Chivilikhin S 2016 On-chip realization of quantum circuits by using waveguides on Si3N4 *J. Phys.: Conf. Ser.* **741** 012104
[23] Jennewein T, Barbieri M and White A G 2011 Single-photon device requirements for operating linear optics quantum computing outside the post-selection basis *J. Mod. Opt.* **58** 276–87
[24] Johansson J R, Nation P D and Nori F 2013 QuTiP 2: a Python framework for the dynamics of open quantum systems *Comput. Phys. Commun.* **184** 1234
[25] Poot M, Schuck C, Ma X, Guo X and Tang H 2016 Design and characterization of integrated components for SiN photonic quantum circuits *Opt. Express* **24** 6843–60
[26] Murphy T 2019 Waveguide Mode Solver MATLAB Central File Exchange (https://mathworks.com/matlabcentral/fileexchange/12734-waveguide-mode-solver)